NANO LETTERS

pubs.acs.org/NanoLett

Letter

Large-Scale Domain Engineering in Two-Dimensional Ferroelectric $CuInP_2S_6$ via Giant Flexoelectric Effect

Chen Chen,[⊥] Heng Liu,[⊥] Qinglin Lai,[⊥] Xiaoyu Mao, Jun Fu, Zhaoming Fu,* and Hualing Zeng*

Cite This: *Nano Lett.* 2022, 22, 3275−3282

Read Online

ACCESS | Metrics & More | Article Recommendations | Supporting Information

ABSTRACT: Room-temperature ferroelectricity in two-dimensional (2D) materials is a potential for developing atomic-scale functional devices. However, as a key step for the technology implementations of 2D ferroelectrics in electronics, the controllable generation of uniform domains remains challenging at the current stage because domain engineering through an external electric field at the 2D limit inevitably leads to large leakage currents and material breakdown. Here, we demonstrate a voltage-free method, the flexoelectric effect, to artificially generate large-scale stripe domains in 2D ferroelectric $CuInP_2S_6$ with single domain lateral size at the scale of several hundred microns. With giant strain gradients ($\sim 10^6$ m^{-1}), we mechanically switch the out-of-plane polarization in ultrathin $CuInP_2S_6$. The flexoelectric control of polarization is understood with a distorted Landau−Ginzburg−Devonshire double well model. Through substrate strain engineering, the stripe domain density is controllable. Our results highlight the potential of developing van der Waals ferroelectrics-based flexible electronics.

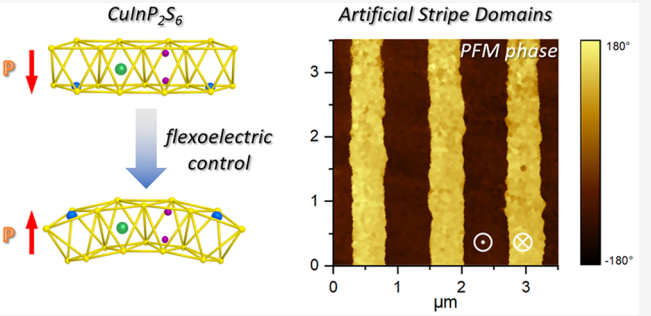

KEYWORDS: *2D ferroelectrics, $CuInP_2S_6$, flexoelectricity, polarization, artificial domains*

Atomically thin van der Waals (vdW) crystals provide the opportunity to explore ferroelectricity at the two-dimensional (2D) limit which is a long-sought goal in conventional bulk ferroelectrics due to the constrain of critical size effect.[1] Experimentally, a series of 2D ferroelectrics with intrinsic either in-plane or out-of-plane electric polarization have been verified, such as the SnTe family,[2−4] $NbOX_2$ family,[5] $CuInP_2S_6$,[6−11] α-In_2Se_3,[12−17] Bi_2O_2Se,[18,19] and d1*T*-$MoTe_2$.[20] Along with the atomic thickness, vdW material also offers the layer degree of freedom that leads to the emergence of sliding ferroelectricity induced by interlayer translation.[21−23] The rich 2D ferroelectricity found in vdW crystals therefore provides the potential to revolutionize future electronic applications with exotic functions.[24−27]

For the integration of 2D ferroelectrics in electronics, how to effectively control the polarization state or ferroelectric domains is the central concern because it fundamentally determines the technical practicability. In bulk ferroelectrics, it can be simply realized by applying an external voltage.[28,29] For example, reliable domain structure in ferroelectric oxide thin film can be artificially created with the aid of a conductive tip in a scanning probe microscope (SPM).[30−32] Nevertheless, for vdW ferroelectrics with atomic thickness the out-of-plane switching electric field at the 2D limit inevitably results in large leakage current and even material breakdown. As a result, the polarization control and especially the large-scale domain generation is relatively challenging in 2D ferroelectrics. Therefore, an alternative method which is free of external voltage is highly in demand for domain manipulation in vdW ferroelectrics.

Here, to address the above issue we utilize the flexoelectric effect, a voltage-free mechanical method, to switch the electric polarization and generate artificial domains at large-scale in ultrathin vdW ferroelectrics. The flexoelectric effect (or flexoelectricity) refers to the formation of net electric polarization inside a crystal when an inhomogeneous strain is applied.[33,34] This effect is universal for all materials with arbitrary lattice symmetry and thus has been utilized to generate many extraordinary phenomena and functionalities such as enhanced piezoelectricity,[35−38] the nanoscale polar vortices,[39] and anomalous photovoltaics.[40−42] To utilize flexoelectricity in polarization reorientation, the key is the generation of giant strain gradients.[43,44] In conventional oxides ferroelectrics, due to the bulk nature with rigid covalence/ionic bond, mechanical domain control is generally realized under the involvement of an SPM tip via nanoscale imprinting or through atomic-scale misfit lattice strain.[43,45−49] For 2D vdW ferroelectrics with genuine mechanical flexibility, the flexo-

Received: January 14, 2022
Revised: April 5, 2022
Published: April 12, 2022

https://doi.org/10.1021/acs.nanolett.2c00130
Nano Lett. 2022, 22, 3275−3282

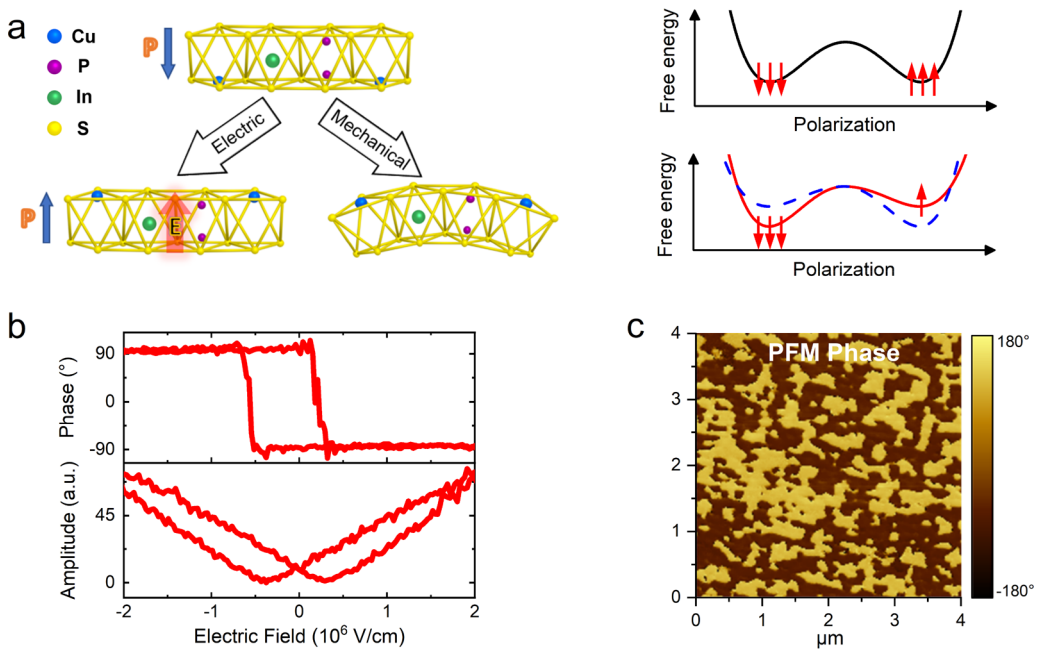

Figure 1. Methods of polarization switching in 2D ferroelectrics. (a) (Left panel) Crystal structure of CIPS and the approaches to switch the polarization. The polarization direction is indicated in by the blue arrows. (Right panel) The corresponding Landau−Ginzburg−Devonshire double well models for ferroelectric phase and polarization switching process. (b) The PFM hysteresis loops and (c) the spontaneous ferroelectric domains from a 14 nm thick CIPS flake.

electric modulating of polarization is relatively easy,[50,51] offering the feasibility of further voltage-free domain engineering at large-scale.

In this work, we demonstrate the mechanical formation of artificial stripe domains in ultrathin $CuInP_2S_6$ (CIPS). The required strain gradients ($\sim 10^6$ m^{-1}) at nanoscale in CIPS was introduced from periodic prestrained substrate. With in situ piezoresponse force microscopy (PFM) measurement, we observed bidirectional modulation of the polarization in rippled CIPS and large ferroelectric domains with single domain lateral size at the order of several hundred microns. The flexoelectric control of polarization in CIPS is understood with a distorted Landau−Ginzburg−Devonshire (LGD) double well model, which is evidenced by the shifted ferroelectric hysteresis loops and the first-principle calculations. Through substrate mechanical strain engineering, the stripe domain density is controllable. Our results highlight the potential of developing vdW ferroelectrics-based flexible 2D electronics.

To begin, we start from the lattice structure of CIPS. As shown in Figure 1a, there are two bonds present: the covalent bonds associated with the $[P_2S_6]^{4-}$ anion sublattice and the ionic bonds associated with the Cu^+ and In^{3+} cation sublattices. The sulfur atoms in the anion sublattice form octahedral cages. One-third of these cages are taken by the P−P dimers supporting this framework; the other two-third are filled by the metal cations with In^{3+} sitting near the center and Cu^+ occupying a trigonal position on an octahedral face near the vdW gap.[52] In each single layer, the atomic position deviation of Cu^+ ions breaks the lattice inversion symmetry, resulting in explicitly out-of-plane ferroelectricity. The two thermodynamically equivalent polarized states in ferroelectrics can be described by the LGD double well model (see Figure 1a). When reversing the polarization, the degeneracy of the ground states should be lifted off via external stimulus such as electric field or inhomogeneous strain (i.e., strain gradients) that lowers the switching energy barrier between the two energy minima. The latter, known as the flexoelectricity effect,[33,34] is with the benefit of voltage-free and large-scale uniformity for 2D vdW ferroelectrics which have atomic scale thickness and ultrahigh flexibility. Therefore, we apply this method to ultrathin CIPS in this study.

CIPS thin flakes were mechanically exfoliated from the bulk and were transferred onto the Au/SiO_2 substrate (detailed in Supporting Information). The single crystal nature of the samples studied here was confirmed by Raman spectroscopy (see Figure S1), where featured phonon modes were observed. The room-temperature ferroelectricity in CIPS can be evidenced from two aspects. As shown in Figure 1b, typical single/butterfly like ferroelectric hysteresis loop in the PFM phase/amplitude spectra were measured from a 20 nm thick CIPS sample. We estimate the coercive field for ultrathin CIPS to be around 3.5×10^5 V/cm. This value is consistent with the results in previous studies.[7] Furthermore, spontaneous domains with unambiguous domain wall structures are clearly visualized in Figure 1c (PFM phase image) and Figure S2b (PFM amplitude image). By carefully examining the domain size, we find that the domains in ultrathin CIPS are fractional with typical area of around 0.2 μm^2 (see Figure S2c). The scattered domains are due to the ferroelectric transition temperature (T_c) of CIPS at ~315 K, which is close to room temperature. Therefore, under ambient conditions strong thermal fluctuation will hinder the formation of large size domains in CIPS. Besides, we also carried out PFM tests on an 18 nm thick CIPS thin flake with 0.5, 1, and 2 V_{AC}, respectively, to exclude the influence of the AC voltage on the ferroelectric domain structures (see Figure S3). We also used the DC electric poling via PFM to check the quality of artificial domains. As shown in Figure S4, a box-in-box pattern has been poled with ±7 V_{DC} tip bias. However, consistent with other

https://doi.org/10.1021/acs.nanolett.2c00130
Nano Lett. 2022, 22, 3275−3282

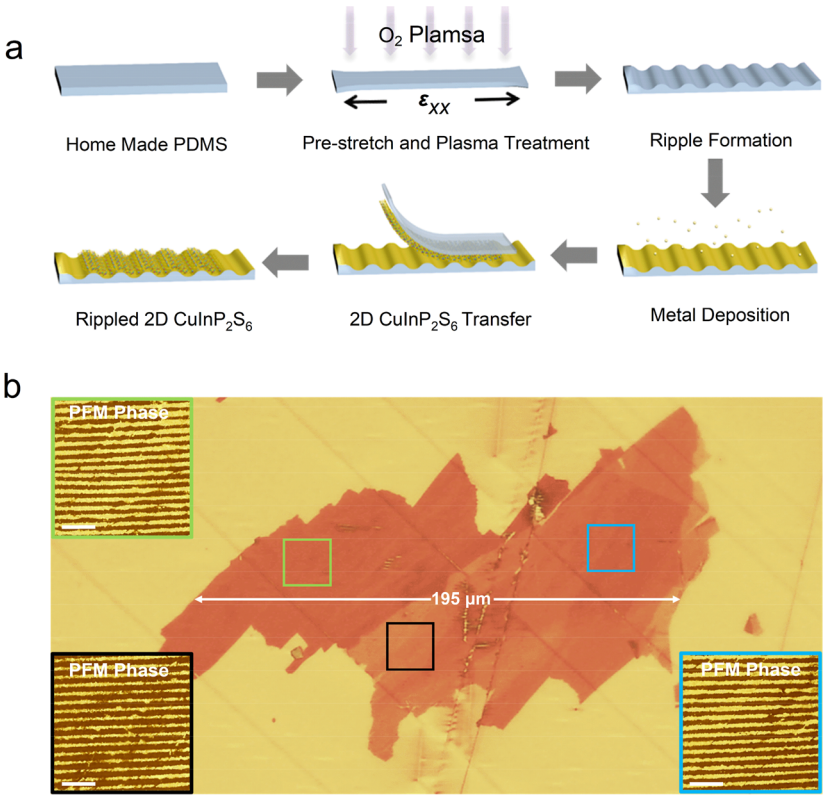

Figure 2. Artificial domain engineering in 2D CIPS via flexoelectricity. (a) Schematic illustration of the fabrication process of the corrugated periodic structure in 2D CIPS. (b) Optical image of the rippled CIPS thin flakes (14−20 nm thickness). The maximum length of the sample along the stripe direction is 195 μm. The insets show the PFM phase images of uniform stripe domains at selected regions, the scale bar represents 5 μm.

reports of electric poling in CIPS,[7,8,11] electric field writing does not guarantee effective switch of all the polarizations as indicated by the poor quality of artificially poled domains.

The key to flexoelectric control of the electric polarization in ferroelectrics is to apply large enough strain gradients, which scale inversely with the dimensionality and the size of materials. Benefitting from the flexural out-of-plane bending mode of ultrathin 2D materials, the giant strain gradients can be introduced in regions with high curvature. Therefore, corrugating the 2D CIPS at nanoscale is a good scenario. As summarized in Figure 2a, we developed a method to create rippled ultrathin CIPS on gold coated polydimethylsiloxane (PDMS) through the combination of substrate strain engineering and the all-dry transfer technique. Details of the corrugating process are described in Supporting Information. With this method, we realized the formation of large area rippled CIPS thin flakes with lateral size at around 195 μm (see the optical image in Figure 2b). The thicknesses of the thin flakes range from 14 to 20 nm (see Figure S5). The polarization states of selected regions with different thicknesses are revealed by the PFM results as shown in the insets of Figure 2b and Figure S6. From the PFM results, we found ordered stripe domains with extremely high uniformity. The formation of uniform stripe ferroelectric domains suggests that the polarization of the entire large area CIPS thin flake can be effectively modulated by the substrate strain engineering at nanoscale. Importantly, artificial domain formation in 2D CIPS via the flexoelectric effect is valid even at scales as large as hundreds of microns.

We next investigate the relationship between the polarization state and the strain gradients ($\partial u/\partial z$). Figure 3a shows the topography of a periodic rippled CIPS with PFM contact mode under low loading force (60 nN). We found two regions with the thicknesses identified to be 4 nm (marked by the green line) and 22 nm (marked by the black line), respectively. By examining the piezoresponse from a single periodic area including both the upward and downward bending, the flexoelectric control on polarization is exclusively confirmed by the observation of domain walls with vanished PFM amplitude and the clear 180° phase contrast between domains as presented in Figure 3b,c, respectively. The boundary in PFM phase image (i.e., domain wall) is consistent with the inflection points in the topography image (see Figure S7). It must be emphasized here, relative to the continuously changing topography, the two plateaus in the phase line profile and the rapid switching behavior imply that the measured PFM phase is not from the crosstalk of surface topography. The optical image and the PFM results of the entire CIPS thin flake are shown in Figure S8. From the PFM results, we clearly observe that the artificial stripe domains (domain walls) were achieved of the entire sample. Because the flexoelectric modulation relies on substrate strain transfer, it is necessary to check the adhesion between the CIPS and the PDMS substrate. Therefore, we extracted the line profiles of height perpendicular to the rippled structure. As shown in Figure 3d, the rippled structure has a near-symmetric double-arc geometry of upward and downward bending. In the region with CIPS samples, there is an offset change in height, which indicates the thickness of the CIPS samples. Meanwhile, the identical depths of the substrate and the samples indicate the good adhesion of the CIPS thin flakes to the substrate. Moreover, we carried out the topography test in tapping mode

https://doi.org/10.1021/acs.nanolett.2c00130
Nano Lett. 2022, 22, 3275−3282

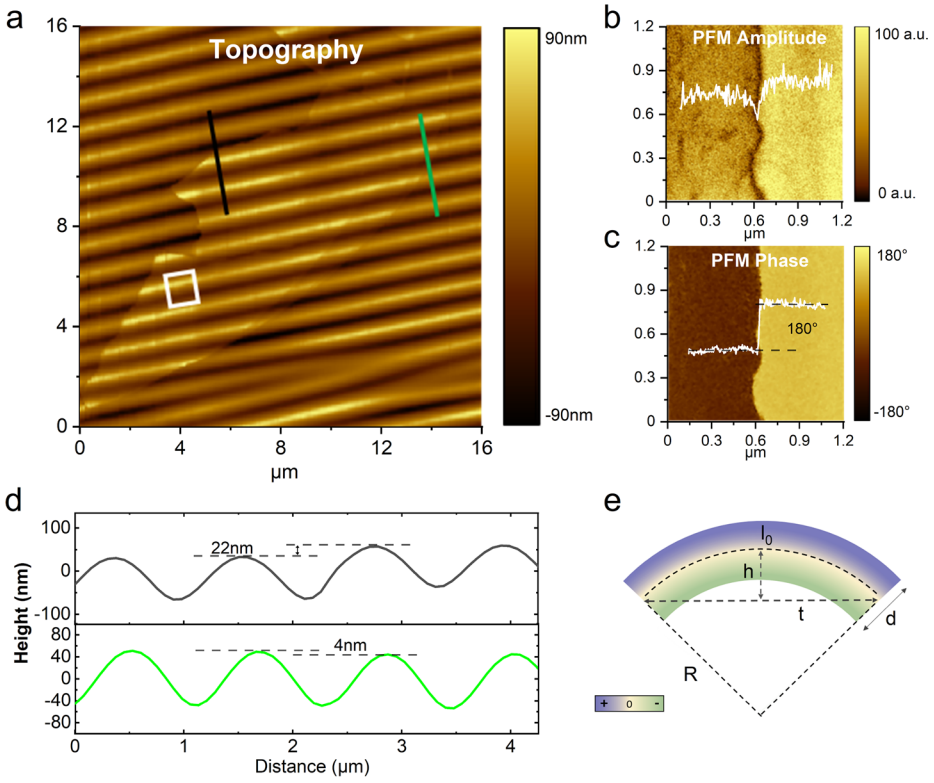

Figure 3. Quantification of the flexoelectric effect in 2D CIPS. (a) Topography image of the rippled CIPS thin flake. Zoomed PFM amplitude (b) and phase (c) images of one period including both upward and downward bending thin CIPS as indicated in the white square region in (a). The insets show the corresponding lateral profiles of amplitude and phase. (d) Selected line profiles of height derived from (a). (e) Simplified arch model for the flexoelectric control of polarization in 2D CIPS. The parameters such as ideal radius of curvature (R), sample thickness (d), wrinkle depth ($2h$), periodicity ($2t$), and original sample length (l_0) can be directly obtained from panel d.

(see Figure S9), in which the same offset changes in height are observed, which guarantees the transfer of the strain.

From the observed tomography, the corrugated periodic structure in CIPS can be simplified into an arch model (see schematic in Figure 3e) by considering the sample bending nature of the flexoelectric control. The geometry parameters of this model are obtained from the in situ morphology measurements. For CIPS thin flakes with a certain thickness d, upon bending, the upper part experiences tensile strain, while the lower part undergoes compressive strain. Thus, the strain gradient $\partial u/\partial z$ is perpendicular to the surface and can be written as[44]

$$\frac{\partial u}{\partial z} \sim \frac{u_1 - u_2}{d} = \frac{\frac{\left(R + \frac{d}{2}\right)\frac{l_0}{R} - l_0}{l_0} - \frac{\left(R - \frac{d}{2}\right)\frac{l_0}{R} - l_0}{l_0}}{d} = \frac{1}{R} \quad (1)$$

where u_1 and u_2 are the in-plane strain of the upper surface and the lower surface respectively, l_0 is the original length of the sample, and R is the ideal radius of curvature of the bended sample. From eq 1, the strain gradient $\partial u/\partial z$ is inversely proportional to R, which can be calculated by the Pythagorean theorem as

$$R = \frac{h^2 + \left(\frac{t}{2}\right)^2}{2h} \quad (2)$$

where h and t are the half of the wrinkle depth and the half of the periodicity. From the height profile in Figure 3d, the h and t are found to be 50 and 600 nm, respectively. In this case, R is calculated to be 925 nm, and $\partial u/\partial z$ is as large as 1.08×10^6 m^{-1}. Compared with previous studies of mechanical bending in bulk materials at macroscopic scale where the strain gradient is usually less than 0.1 m^{-1},[42,53,54] our result achieves a strain gradient of 10^6 m^{-1}. Although the applied strain gradient is giant in this study, the ultrathin CIPS samples remain intact other than collapse. This is benefited from the unique near-zero Poisson ratio found in CIPS,[55] so there is almost no out-of-plane strain in our bending geometry. Meanwhile, the in-plane strain in CIPS thin layers (the top and the bottom) is around ±1%.

With the quantified strain gradients, we can estimate the value of effective flexoelectric field, E_{flexo}. The flexoelectric field can be expressed as[33,43,44]

$$E_{flexo} = \frac{P_{flexo}}{\varepsilon_r \varepsilon_0} = \frac{1}{\varepsilon_r \varepsilon_0}\left(\mu \frac{\partial u}{\partial z}\right) \quad (3)$$

where ε_0 is the permittivity of free space and ε_r is relative dielectric permittivity, P_{flexo} is the polarization induced by flexoelectricity, and μ is the flexoelectric coefficient. According to Tagantsev's phenomenological studies of the flexoelectric effect in crystalline materials, μ can be approximately expressed as[33,34]

$$\mu \sim \chi \frac{e}{a} \quad (4)$$

where χ is the dielectric susceptibility ($\chi = \varepsilon_r - 1 \approx \varepsilon_r$), e is the electron charge, and a is the lattice constant. For CIPS, the ε_r is 40 and a is 6×10^{-10} m.[55] We have the flexoelectric coefficient μ to be 10.8 nC/m. Therefore, the flexoelectric field E_{flexo} in the rippled structure is around 3×10^5 V/cm. The strength of

https://doi.org/10.1021/acs.nanolett.2c00130
Nano Lett. 2022, 22, 3275−3282

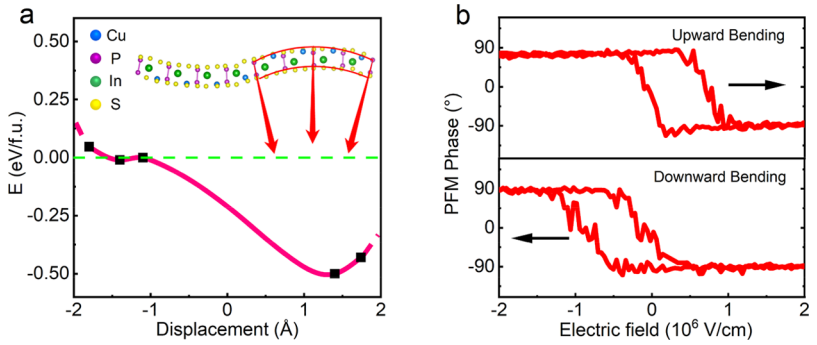

Figure 4. The distorted LGD model for the flexoelectric switch of polarization. (a) Calculated potential energy profiles with asymmetric double-well potential for bended CIPS. The inset shows the side view of the corrugated crystal structures of 2D CIPS with the out-of-plane strain gradients displayed by red arrows. (b) Shifted PFM hysteresis loops measured from the upward and downward bending region.

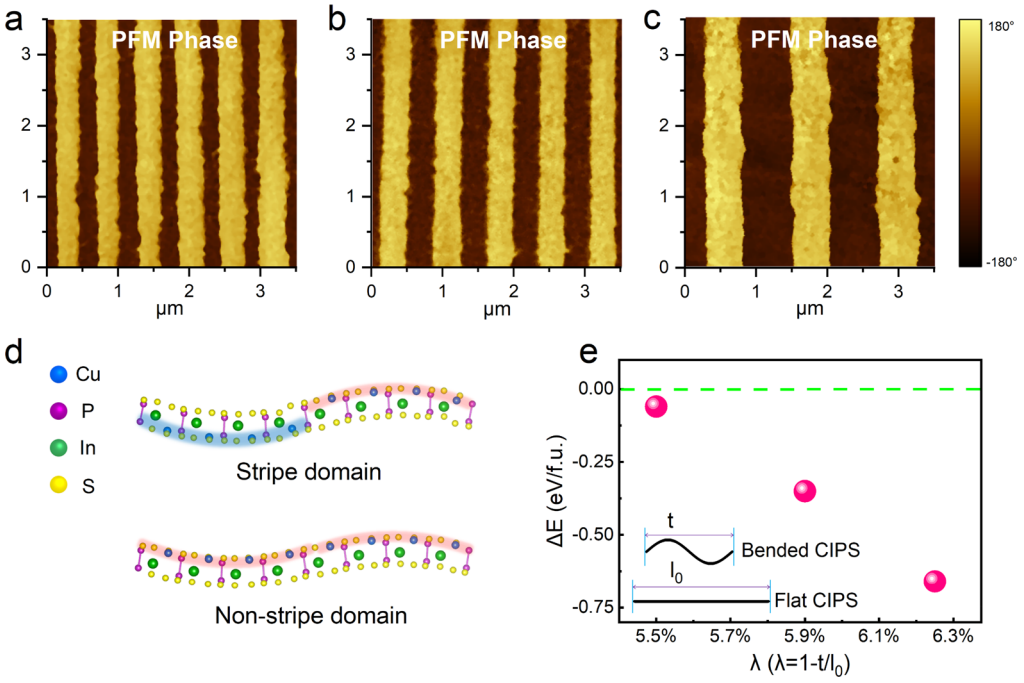

Figure 5. Controlled stripe domain generation in 2D CIPS. (a–c) The stripe domains with varied periodicities. The periodicity is 530, 705, and 1200 nm, respectively. (d) Side view of the corrugated crystal structures of CIPS flakes with and without stripe domains. The positions of Cu^+ ions are highlighted to distinguish the strip domain and single domain. (e) Comparison between the lattice stabilities of corrugated CIPS strip domain and single domain. The inset shows the degree of bending, which is depicted by a scale factor $\lambda = 1 - t/l_0$, where l_0 and t are the length of flat and corrugated supercell including the same number of unit cells, respectively.

the flexoelectric field is comparable to the coercive field of CIPS nanoflakes extracted from the hysteresis loops measurement (~3.5 × 10^5 V/cm) and in a previous report.[7] It further proves the validity of flexoelectric modulation on the electric polarizations of CIPS in this study. Furthermore, it should be pointed out that the flexoelectric coefficients μ of ferroelectric materials is temperature dependent and should increase largely near the Curie temperature T_c.[56] Because the T_c of CIPS is ~315 K, which is close to the room temperature,[9] the flexoelectric coefficients μ and the flexoelectric field E_{flexo} in our bending geometry under ambient conditions may be much larger than we estimated.

The geometry-induced flexoelectric effect in 2D CIPS can be understood through the distorted LGD double-well potential model. As a phenomenological theory, it is often employed to qualitatively explain the flexoelectric effect in ferroelectrics. Here, the potential energy profiles (PEP) are quantificationally obtained for CIPS system based on first-principle calculations as shown in Figure 4a. The details of calculation methods and models are given in Supporting Information. For both the flat and bended CIPSs, the migration barriers of Cu^+ from one surface to the other surface are calculated (see Figure 4a and Figure S11). It is found that the PEP of the flat CIPS has a symmetric double well for the migration of Cu^+ (see Figure S11); the PEP of the bended CIPS also has a double-well structure but is asymmetric (see Figure 4a). Obviously, it is the strain gradients that break the symmetry of potential energy surface. These calculated results are consistent with the phenomenological theory. It is worth noting that in bended CIPS the migration barrier of Cu^+ from the contraction surface to stretched surface is much smaller than that between upper and lower surfaces in flat CIPS.

The distorted LGD double-well potential model can be verified through the ferroelectric switching behavior of rippled

https://doi.org/10.1021/acs.nanolett.2c00130
Nano Lett. 2022, 22, 3275−3282

CIPS nanoflakes via single electric poling measurements. Figure 4b shows the hysteresis loops from the downward and upward bending areas of a 14 nm thick CIPS, respectively. Because of the symmetrical geometry, downward and upward bending regions should have the same coercivity. The coercive field which is equal to the half-width of the hysteresis loop was found to be around 3.7×10^5 V/cm at both of downward and upward bending regions, which is close to the value we estimated above. Importantly, the hysteresis loops of downward/upward bending regions are entirely shifted to the negative/positive voltage range accordingly. This result suggests that the degenerate electric polarizations in CIPS are not stable in the bending state. Only either up or down electric polarization can be stabilized subject to the bending direction, which is the manifestation of the flexoelectric effect.[43] When the flexoelectric field induced by strain gradients is parallel to the ferroelectric polarization, it could increase the required external coercive voltage. On the contrary, the flexoelectric field would decrease the required external coercive voltage.

Finally, we show that the stripe domains in 2D CIPS can be effectively tuned in density with the developed substrate strain engineering technique. Controlled arrays of domains in ferroelectrics are important for the practical applications such as nonlinear optics, anomalous photovoltaic effect, and so forth. In this study, the stripe domains in CIPS are controlled by the periodicity of the rippled substrate. By adjusting the periodicity of the rippled substrate (detailed in Supporting Information), we generated different stripe domains with periodicities of 530, 750, and 1200 nm, respectively, as shown in Figure 5a−c (the corresponding topography and PFM amplitude image is shown in Figure S12). It should be noted that although the depth of the ripples changed along with the periodicity, the corresponding strain gradients do not change drastically and remain at the order of 1×10^6 m^{-1} which ensures the reversal of the polarization (see Figure S13).

The formation and control of stripe domains in CIPS can be numerically interpreted. We compared the energies with and without stripe domain for the same corrugated structures of CIPS, denoted by E_{Stripe} and $E_{Nonstripe}$, respectively. The calculated energy differences ($\Delta E = E_{Stripe} - E_{Nonstripe}$) are given in Figure 5e. The structures with and without stripe domain are shown by the sketch in Figure 5d. The degree of bending strain can be depicted by a scale factor $\lambda = 1 - t/l_0$, where l_0 and t are the length of flat and corrugated supercell including the same number of unit cells, respectively (see the inset in Figure 5e). This scale factor determines the density of stripe domains. In stripe domains with periodicity of 1200 nm, the corresponding scale factor (λ) is 6.1%, being in the range of our simulated λ values (see Figure 5e). According to the definition of ΔE, the negative values of ΔE indicate that the formation of stripe domain is more preferred in energy. Furthermore, in the structure with stripe domains the Cu ions always prefer to locate at the stretched surface (see Figure 5d) instead of the contraction surface. The latter case corresponds to a metastable state with a higher energy compared to the former, according to calculations. These polarization behaviors are attributed to the flexoelectric effect of ferroelectric CIPS. The evolution trend of ΔE along the λ (or density) indicates that the relative stability of stripe structures increases with the curvature degree of corrugated CIPS.

In summary, we report the flexoelectric method to artificially generate large-scale stripe domains in 2D ferroelectric $CuInP_2S_6$. Giant strain gradient ($\sim 10^6$ m^{-1}) at nanoscale is achieved via substrate engineering. The electric polarizations in ultrathin $CuInP_2S_6$ are mechanically switched via nanoscale bending. Together with first-principle calculations, the flexoelectric control of ferroelectric polarization in 2D CIPS is verified via distorted LGD double well model. Our work highlights the potential of developing vdW ferroelectrics-based flexible 2D electronics.

■ ASSOCIATED CONTENT

Supporting Information

The Supporting Information is available free of charge at https://pubs.acs.org/doi/10.1021/acs.nanolett.2c00130.

Additional results and details for substrate formation, sample preparation, Raman spectroscopy characterization, PFM characterization, first-principle calculation methods, dependence of strain gradients on the periodicity of domains, polarization of the rippled CIPS thin flake, effect of the strain gradients on the T_c of ferroelectric CIPS, outlook for reconfigurable flexoelectric modulation in 2D CIPS (PDF)

■ AUTHOR INFORMATION

Corresponding Authors

Zhaoming Fu − *College of Physics and Electronic Information, Yunnan Normal University, Kunming 650500, China; Yunnan Key Laboratory of Optoelectronic Information Technology, Kunming 650500, China*; Email: fuzhm1979@163.com

Hualing Zeng − *International Center for Quantum Design of Functional Materials (ICQD), Hefei National Laboratory for Physical Science at the Microscale and Key Laboratory of Strongly-Coupled Quantum Matter Physics, Chinese Academy of Sciences, Department of Physics, University of Science and Technology of China, Hefei, Anhui 230026, People's Republic of China*; orcid.org/0000-0001-5869-9553; Email: hlzeng@ustc.edu.cn

Authors

Chen Chen − *International Center for Quantum Design of Functional Materials (ICQD), Hefei National Laboratory for Physical Science at the Microscale and Key Laboratory of Strongly-Coupled Quantum Matter Physics, Chinese Academy of Sciences, Department of Physics, University of Science and Technology of China, Hefei, Anhui 230026, People's Republic of China*

Heng Liu − *International Center for Quantum Design of Functional Materials (ICQD), Hefei National Laboratory for Physical Science at the Microscale and Key Laboratory of Strongly-Coupled Quantum Matter Physics, Chinese Academy of Sciences, Department of Physics, University of Science and Technology of China, Hefei, Anhui 230026, People's Republic of China*

Qinglin Lai − *International Center for Quantum Design of Functional Materials (ICQD), Hefei National Laboratory for Physical Science at the Microscale and Key Laboratory of Strongly-Coupled Quantum Matter Physics, Chinese Academy of Sciences, Department of Physics, University of Science and Technology of China, Hefei, Anhui 230026, People's Republic of China*

Xiaoyu Mao − *International Center for Quantum Design of Functional Materials (ICQD), Hefei National Laboratory for*

https://doi.org/10.1021/acs.nanolett.2c00130
Nano Lett. 2022, 22, 3275−3282

Physical Science at the Microscale and Key Laboratory of Strongly-Coupled Quantum Matter Physics, Chinese Academy of Sciences, Department of Physics, University of Science and Technology of China, Hefei, Anhui 230026, People's Republic of China; orcid.org/0000-0003-0849-2436

Jun Fu − *International Center for Quantum Design of Functional Materials (ICQD), Hefei National Laboratory for Physical Science at the Microscale and Key Laboratory of Strongly-Coupled Quantum Matter Physics, Chinese Academy of Sciences, Department of Physics, University of Science and Technology of China, Hefei, Anhui 230026, People's Republic of China*

Complete contact information is available at: https://pubs.acs.org/10.1021/acs.nanolett.2c00130

Author Contributions

⊥C.C., H.L., and Q.L. contributed equally to this work.

Author Contributions

H.Z. conceived the idea and supervised the research. C.C., H.L., and Q.L. prepared the samples, fabricated the devices, and carried out the PFM measurements. C.C., Z.F., and H.Z. analyzed the data and wrote the paper. All authors commented on the manuscript.

Notes

The authors declare no competing financial interest.

■ ACKNOWLEDGMENTS

This work was supported by the National Key Research and Development Program of China (Grant 2017YFA0205004), the National Natural Science Foundation of China (Grant 11674295), the Fundamental Research Funds for the Central Universities (Grants WK2030020032 and WK3510000013), and the Anhui Initiative in Quantum Information Technologies (Grant AHY170000). This work was partially carried out at the USTC Center for Micro and Nanoscale Research and Fabrication.

■ REFERENCES

(1) Junquera, J.; Ghosez, P. Critical thickness for ferroelectricity in perovskite ultrathin films. *Nature* **2003**, *422* (6931), 506−509.

(2) Chang, K.; Liu, J.; Lin, H.; Wang, N.; Zhao, K.; Zhang, A.; Jin, F.; Zhong, Y.; Hu, X.; Duan, W.; Zhang, Q.; Fu, L.; Xue, Q.-K.; Chen, X.; Ji, S.-H. Discovery of robust in-plane ferroelectricity in atomic-thick SnTe. *Science* **2016**, *353* (6296), 274−278.

(3) Bao, Y.; Song, P.; Liu, Y.; Chen, Z.; Zhu, M.; Abdelwahab, I.; Su, J.; Fu, W.; Chi, X.; Yu, W.; Liu, W.; Zhao, X.; Xu, Q.-H.; Yang, M.; Loh, K. P. Gate-tunable in-plane ferroelectricity in few-layer SnS. *Nano Lett.* **2019**, *19* (8), 5109−5117.

(4) Higashitarumizu, N.; Kawamoto, H.; Lee, C.-J.; Lin, B.-H.; Chu, F.-H.; Yonemori, I.; Nishimura, T.; Wakabayashi, K.; Chang, W.-H.; Nagashio, K. Purely in-plane ferroelectricity in monolayer SnS at room temperature. *Nat. Commun.* **2020**, *11* (1), 1−9.

(5) Jia, Y.; Zhao, M.; Gou, G.; Zeng, X. C.; Li, J. Niobium oxide dihalides $NbOX_2$: a new family of two-dimensional van der Waals layered materials with intrinsic ferroelectricity and antiferroelectricity. *Nanoscale Horiz.* **2019**, *4* (5), 1113−1123.

(6) Deng, J.; Liu, Y.; Li, M.; Xu, S.; Lun, Y.; Lv, P.; Xia, T.; Gao, P.; Wang, X.; Hong, J. Thickness-Dependent In-Plane Polarization and Structural Phase Transition in van der Waals Ferroelectric $CuInP_2S_6$. *Small* **2020**, *16* (1), 1904529.

(7) Liu, F.; You, L.; Seyler, K. L.; Li, X.; Yu, P.; Lin, J.; Wang, X.; Zhou, J.; Wang, H.; He, H.; Pantelides, S. T.; Zhou, W.; Sharma, P.; Xu, X.; Ajayan, P. M.; Wang, J.; Liu, Z. Room-temperature ferroelectricity in $CuInP_2S_6$ ultrathin flakes. *Nat. Commun.* **2016**, *7* (1), 1−6.

(8) Xu, D.-D.; Ma, R.-R.; Fu, A.-P.; Guan, Z.; Zhong, N.; Peng, H.; Xiang, P.-H.; Duan, C.-G. Ion adsorption-induced reversible polarization switching of a van der Waals layered ferroelectric. *Nat. Commun.* **2021**, *12* (1), 1−9.

(9) Belianinov, A.; He, Q.; Dziaugys, A.; Maksymovych, P.; Eliseev, E.; Borisevich, A.; Morozovska, A.; Banys, J.; Vysochanskii, Y.; Kalinin, S. V. $CuInP_2S_6$ room temperature layered ferroelectric. *Nano Lett.* **2015**, *15* (6), 3808−3814.

(10) Zhang, D.; Luo, Z.-D.; Yao, Y.; Schoenherr, P.; Sha, C.; Pan, Y.; Sharma, P.; Alexe, M.; Seidel, J. Anisotropic Ion Migration and Electronic Conduction in van der Waals Ferroelectric $CuInP_2S_6$. *Nano Lett.* **2021**, *21* (2), 995−1002.

(11) Balke, N.; Neumayer, S. M.; Brehm, J. A.; Susner, M. A.; Rodriguez, B. J.; Jesse, S.; Kalinin, S. V.; Pantelides, S. T.; McGuire, M. A.; Maksymovych, P. Locally controlled Cu-ion transport in layered ferroelectric $CuInP_2S_6$. *ACS Appl. Mater. Interfaces* **2018**, *10* (32), 27188−27194.

(12) Ding, W.; Zhu, J.; Wang, Z.; Gao, Y.; Xiao, D.; Gu, Y.; Zhang, Z.; Zhu, W. Prediction of intrinsic two-dimensional ferroelectrics in In_2Se_3 and other III_2-VI_3 van der Waals materials. *Nat. Commun.* **2017**, *8* (1), 1−8.

(13) Zhou, Y.; Wu, D.; Zhu, Y.; Cho, Y.; He, Q.; Yang, X.; Herrera, K.; Chu, Z.; Han, Y.; Downer, M. C.; Peng, H.; Lai, K. Out-of-plane piezoelectricity and ferroelectricity in layered α- In_2Se_3 nanoflakes. *Nano Lett.* **2017**, *17* (9), 5508−5513.

(14) Cui, C.; Hu, W.-J.; Yan, X.; Addiego, C.; Gao, W.; Wang, Y.; Wang, Z.; Li, L.; Cheng, Y.; Li, P.; Zhang, X.; Alshareef, H. N.; Wu, T.; Zhu, W.; Pan, X.; Li, L.-J. Intercorrelated in-plane and out-of-plane ferroelectricity in ultrathin two-dimensional layered semiconductor In_2Se_3. *Nano Lett.* **2018**, *18* (2), 1253−1258.

(15) Zheng, C.; Yu, L.; Zhu, L.; Collins, J. L.; Kim, D.; Lou, Y.; Xu, C.; Li, M.; Wei, Z.; Zhang, Y.; Edmonds, M. T.; Li, S.; Seidel, J.; Zhu, Y.; Liu, J. Z.; Tang, W.-X.; Fuhrer, M. S. Room temperature in-plane ferroelectricity in van der Waals In_2Se_3. *Sci. Adv.* **2018**, *4* (7), eaar7720.

(16) Xiao, J.; Zhu, H.; Wang, Y.; Feng, W.; Hu, Y.; Dasgupta, A.; Han, Y.; Wang, Y.; Muller, D. A.; Martin, L. W.; Hu, P.; Zhang, X. Intrinsic two-dimensional ferroelectricity with dipole locking. *Phys. Rev. Lett.* **2018**, *120* (22), 227601.

(17) Wan, S.; Li, Y.; Li, W.; Mao, X.; Zhu, W.; Zeng, H. Room-temperature ferroelectricity and a switchable diode effect in two-dimensional α- In_2Se_3 thin layers. *Nanoscale* **2018**, *10* (31), 14885−14892.

(18) Wu, M.; Zeng, X. C. Bismuth oxychalcogenides: a new class of ferroelectric/ferroelastic materials with ultra high mobility. *Nano Lett.* **2017**, *17* (10), 6309−6314.

(19) Ghosh, T.; Samanta, M.; Vasdev, A.; Dolui, K.; Ghatak, J.; Das, T.; Sheet, G.; Biswas, K. Ultrathin free-standing nanosheets of Bi_2O_2Se: room temperature ferroelectricity in self-assembled charged layered heterostructure. *Nano Lett.* **2019**, *19* (8), 5703−5709.

(20) Yuan, S.; Luo, X.; Chan, H. L.; Xiao, C.; Dai, Y.; Xie, M.; Hao, J. Room-temperature ferroelectricity in $MoTe_2$ down to the atomic monolayer limit. *Nat. Commun.* **2019**, *10* (1), 1−6.

(21) Fei, Z.; Zhao, W.; Palomaki, T. A.; Sun, B.; Miller, M. K.; Zhao, Z.; Yan, J.; Xu, X.; Cobden, D. H. Ferroelectric switching of a two-dimensional metal. *Nature* **2018**, *560* (7718), 336−339.

(22) Yasuda, K.; Wang, X.; Watanabe, K.; Taniguchi, T.; Jarillo-Herrero, P. Stacking-engineered ferroelectricity in bilayer boron nitride. *Science* **2021**, *372* (6549), 1458−1462.

(23) Li, L.; Wu, M. Binary compound bilayer and multilayer with vertical polarizations: two-dimensional ferroelectrics, multiferroics, and nanogenerators. *ACS Nano* **2017**, *11* (6), 6382−6388.

(24) Dai, M.; Wang, Z.; Wang, F.; Qiu, Y.; Zhang, J.; Xu, C.-Y.; Zhai, T.; Cao, W.; Fu, Y.; Jia, D.; Zhou, Y.; Hu, P.-A. Two-Dimensional van der Waals Materials with aligned in-plane polarization and large piezoelectric effect for self-powered piezoelectric sensors. *Nano Lett.* **2019**, *19* (8), 5410−5416.

(25) Si, M.; Saha, A. K.; Gao, S.; Qiu, G.; Qin, J.; Duan, Y.; Jian, J.; Niu, C.; Wang, H.; Wu, W.; Gupta, S. K.; Ye, P. D. A ferroelectric semiconductor field-effect transistor. *Nat. Electron.* **2019**, *2* (12), 580−586.
(26) Wang, S.; Liu, L.; Gan, L.; Chen, H.; Hou, X.; Ding, Y.; Ma, S.; Zhang, D. W.; Zhou, P. Two-dimensional ferroelectric channel transistors integrating ultra-fast memory and neural computing. *Nat. Commun.* **2021**, *12* (1), 1−9.
(27) Wu, J.; Chen, H.-Y.; Yang, N.; Cao, J.; Yan, X.; Liu, F.; Sun, Q.; Ling, X.; Guo, J.; Wang, H. High tunnelling electroresistance in a ferroelectric van der Waals heterojunction via giant barrier height modulation. *Nat. Electron.* **2020**, *3* (8), 466−472.
(28) Dawber, M.; Rabe, K.; Scott, J. Physics of thin-film ferroelectric oxides. *Rev. Mod. Phys.* **2005**, *77* (4), 1083.
(29) Scott, J. F.; Paz de Araujo, C. A. Ferroelectric memories. *Science* **1989**, *246* (4936), 1400−1405.
(30) Choi, T.; Lee, S.; Choi, Y.; Kiryukhin, V.; Cheong, S.-W. Switchable ferroelectric diode and photovoltaic effect in $BiFeO_3$. *Science* **2009**, *324* (5923), 63−66.
(31) Catalan, G.; Béa, H.; Fusil, S.; Bibes, M.; Paruch, P.; Barthélémy, A.; Scott, J. Fractal dimension and size scaling of domains in thin films of multiferroic $BiFeO_3$. *Phys. Rev. Lett.* **2008**, *100* (2), 027602.
(32) Lipatov, A.; Li, T.; Vorobeva, N. S.; Sinitskii, A.; Gruverman, A. Nanodomain engineering for programmable ferroelectric devices. *Nano Lett.* **2019**, *19* (5), 3194−3198.
(33) Zubko, P.; Catalan, G.; Tagantsev, A. K. Flexoelectric effect in solids. *Annu. Rev. Mater. Res.* **2013**, *43*, 387−421.
(34) Nguyen, T. D.; Mao, S.; Yeh, Y. W.; Purohit, P. K.; McAlpine, M. C. Nanoscale flexoelectricity. *Adv. Mater.* **2013**, *25* (7), 946−974.
(35) Kang, S.; Jeon, S.; Kim, S.; Seol, D.; Yang, H.; Lee, J.; Kim, Y. Tunable out-of-plane piezoelectricity in thin-layered $MoTe_2$ by surface corrugation-mediated flexoelectricity. *ACS Appl. Mater. Interfaces* **2018**, *10* (32), 27424−27431.
(36) Wang, X.; Cui, A.; Chen, F.; Xu, L.; Hu, Z.; Jiang, K.; Shang, L.; Chu, J. Probing Effective Out-of-Plane Piezoelectricity in van der Waals Layered Materials Induced by Flexoelectricity. *Small* **2019**, *15* (46), 1903106.
(37) Qi, Y.; Kim, J.; Nguyen, T. D.; Lisko, B.; Purohit, P. K.; McAlpine, M. C. Enhanced piezoelectricity and stretchability in energy harvesting devices fabricated from buckled PZT ribbons. *Nano Lett.* **2011**, *11* (3), 1331−1336.
(38) Yang, Q.; Li, Q.; Liu, Z.; Wang, D.; Guo, Y.; Li, X.; Tang, Y.; Li, H.; Dong, B.; Zhi, C. Periodic Wrinkle-Patterned Single-Crystalline Ferroelectric Oxide Membranes with Enhanced Piezoelectricity. *Adv. Mater.* **2020**, *32* (50), 2004477.
(39) Li, Q.; Nelson, C.; Hsu, S.-L.; Damodaran, A.; Li, L.-L.; Yadav, A.; McCarter, M.; Martin, L.; Ramesh, R.; Kalinin, S. Quantification of flexoelectricity in $PbTiO_3/SrTiO_3$ superlattice polar vortices using machine learning and phase-field modeling. *Nat. Commun.* **2017**, *8* (1), 1−8.
(40) Yang, M.-M.; Kim, D. J.; Alexe, M. Flexo-photovoltaic effect. *Science* **2018**, *360* (6391), 904−907.
(41) Jiang, J.; Chen, Z.; Hu, Y.; Xiang, Y.; Zhang, L.; Wang, Y.; Wang, G.-C.; Shi, J. Flexo-photovoltaic effect in MoS_2. *Nat. Nanotechnol.* **2021**, *16* (8), 894−901.
(42) Shu, L.; Ke, S.; Fei, L.; Huang, W.; Wang, Z.; Gong, J.; Jiang, X.; Wang, L.; Li, F.; Lei, S.; Rao, Z.; Zhou, Y.; Zheng, R.-K.; Yao, X.; Wang, Y.; Stengel, M.; Catalan, G. Photoflexoelectric effect in halide perovskites. *Nat. Mater.* **2020**, *19* (6), 605−609.
(43) Lee, D.; Yoon, A.; Jang, S.; Yoon, J.-G.; Chung, J.-S.; Kim, M.; Scott, J.; Noh, T. Giant flexoelectric effect in ferroelectric epitaxial thin films. *Phys. Rev. Lett.* **2011**, *107* (5), 057602.
(44) Lee, D. Flexoelectricity in thin films and membranes of complex oxides. *APL Mater.* **2020**, *8* (9), 090901.
(45) Lu, H.; Bark, C.-W.; Esque De Los Ojos, D.; Alcala, J.; Eom, C.-B.; Catalan, G.; Gruverman, A. Mechanical writing of ferroelectric polarization. *Science* **2012**, *336* (6077), 59−61.
(46) Celano, U.; Popovici, M.; Florent, K.; Lavizzari, S.; Favia, P.; Paulussen, K.; Bender, H.; di Piazza, L.; Van Houdt, J.; Vandervorst, W. The flexoelectric effect in Al-doped hafnium oxide. *Nanoscale* **2018**, *10* (18), 8471−8476.
(47) Wang, B.; Lu, H.; Bark, C. W.; Eom, C.-B.; Gruverman, A.; Chen, L.-Q. Mechanically induced ferroelectric switching in $BaTiO_3$ thin films. *Acta Mater.* **2020**, *193*, 151−162.
(48) Dong, G.; Li, S.; Yao, M.; Zhou, Z.; Zhang, Y.-Q.; Han, X.; Luo, Z.; Yao, J.; Peng, B.; Hu, Z.; Huang, H.; Jia, T.; Li, J.; Ren, W.; Ye, Z.-G.; Ding, X.; Sun, J.; Nan, C.-W.; Chen, L.-Q.; Li, J.; Liu, M. Super-elastic ferroelectric single-crystal membrane with continuous electric dipole rotation. *Science* **2019**, *366* (6464), 475−479.
(49) Peng, B.; Peng, R.-C.; Zhang, Y.-Q.; Dong, G.; Zhou, Z.; Zhou, Y.; Li, T.; Liu, Z.; Luo, Z.; Wang, S.; Xia, Y.; Qiu, R.; Cheng, X.; Xue, F.; Hu, Z.; Ren, W.; Ye, Z.-G.; Chen, L.-Q.; Shan, Z.; Min, T.; Liu, M. Phase transition enhanced superior elasticity in freestanding single-crystalline multiferroic $BiFeO_3$ membranes. *Sci. Adv.* **2020**, *6* (34), eaba5847.
(50) Qi, L.; Ruan, S.; Zeng, Y. J. Review on recent developments in 2D ferroelectrics: Theories and applications. *Adv. Mater.* **2021**, *33* (13), 2005098.
(51) Yang, Y.; Zong, H.; Sun, J.; Ding, X. Rippling ferroic phase transition and domain switching in 2D materials. *Adv. Mater.* **2021**, *33* (49), 2103469.
(52) Maisonneuve, V.; Cajipe, V.; Simon, A.; Von Der Muhll, R.; Ravez, J. Ferrielectric ordering in lamellar $CuInP_2S_6$. *Phys. Rev. B* **1997**, *56* (17), 10860.
(53) Ma, W.; Cross, L. E. Strain-gradient-induced electric polarization in lead zirconate titanate ceramics. *Appl. Phys. Lett.* **2003**, *82* (19), 3293−3295.
(54) Zubko, P.; Catalan, G.; Buckley, A.; Welche, P.; Scott, J. Strain-gradient-induced polarization in $SrTiO_3$ single crystals. *Phys. Rev. Lett.* **2007**, *99* (16), 167601.
(55) You, L.; Zhang, Y.; Zhou, S.; Chaturvedi, A.; Morris, S. A.; Liu, F.; Chang, L.; Ichinose, D.; Funakubo, H.; Hu, W.; Wu, T.; Liu, Z.; Dong, S.; Wang, J. Origin of giant negative piezoelectricity in a layered van der Waals ferroelectric. *Sci. Adv.* **2019**, *5* (4), eaav3780.
(56) Ma, W.; Cross, L. E. Flexoelectricity of barium titanate. *Appl. Phys. Lett.* **2006**, *88* (23), 232902.

https://doi.org/10.1021/acs.nanolett.2c00130
Nano Lett. 2022, 22, 3275−3282